

Metasurfaces for manipulating surface plasmons

Yongmin Liu and Xiang Zhang

Citation: *Applied Physics Letters* **103**, 141101 (2013); doi: 10.1063/1.4821444

View online: <http://dx.doi.org/10.1063/1.4821444>

View Table of Contents: <http://scitation.aip.org/content/aip/journal/apl/103/14?ver=pdfcov>

Published by the [AIP Publishing](#)

Articles you may be interested in

[Modal and transient analysis of membrane acoustic metasurfaces](#)

J. Appl. Phys. **117**, 045308 (2015); 10.1063/1.4906549

[Dispersion characteristics of surface plasmon polariton modes in a metallic slab waveguide with nonlinear magnetic cladding](#)

J. Appl. Phys. **114**, 214311 (2013); 10.1063/1.4838535

[Optimizing terahertz surface plasmons of a monolayer graphene and a graphene parallel plate waveguide using one-dimensional photonic crystal](#)

J. Appl. Phys. **114**, 033102 (2013); 10.1063/1.4813415

[Direct mapping of surface plasmon dispersion using imaging scatterometry](#)

Appl. Phys. Lett. **102**, 251107 (2013); 10.1063/1.4812482

[Bidirectional bending splitter of designer surface plasmons](#)

Appl. Phys. Lett. **99**, 111904 (2011); 10.1063/1.3639277



Metasurfaces for manipulating surface plasmons

Yongmin Liu^{1,2,3} and Xiang Zhang^{1,a)}

¹NSF Nanoscale Science and Engineering Center (NSEC), 3112 Etcheverry Hall, University of California, Berkeley, California 94720, USA

²Department of Mechanical and Industrial Engineering, Northeastern University, 360 Huntington Avenue, Boston, Massachusetts 02115, USA

³Department of Electrical and Computer Engineering, Northeastern University, 360 Huntington Avenue, Boston, Massachusetts 02115, USA

(Received 7 April 2013; accepted 1 September 2013; published online 30 September 2013)

Metasurfaces have recently emerged as an innovative approach to control light propagation with unprecedented capabilities. Different from previous work concentrating on steering far-field propagating waves, here we demonstrate that metallic metasurfaces can efficiently and effectively manipulate surface plasmons in the near-field regime. By engineering the dispersion of surface plasmons on a simple grating structure, we are able to realize normal, non-divergent as well as anomalous diffraction of surface plasmons. In particular, all-angle and broadband negative refraction of surface plasmons is achieved, largely attributed to the uniquely designed hyperbolic constant frequency contour of surface plasmons propagating along the metasurface. © 2013 AIP Publishing LLC. [<http://dx.doi.org/10.1063/1.4821444>]

Metamaterials are a special type of artificial materials with engineered subwavelength structures. Through regulating the interaction between light and the artificial structures, metamaterials have enabled a host of striking materials properties, including artificial magnetism, tunable electric permittivity, negative refractive indices, extremely large refractive indices, and strong chirality.^{1–3} Such remarkable properties have allowed us to manipulate light propagation in an unparalleled manner. Examples include negative refraction,⁴ reversed Cherenkov radiation,⁵ and invisibility cloaks,^{6,7} to name a few. Thanks to the advanced electromagnetic theories and numerical modeling techniques, state-of-the-art fabrication tools as well as greatly improved characterization and analysis methods, tremendous progress has been achieved in the fascinating field of metamaterials. The operation wavelength of metamaterials has been expanded across a broad electromagnetic spectrum from microwave and terahertz, to infrared and visible. The dimension of metamaterials has also been extended from single layer to bulk (with respect to the wavelength of interest).

Very recently, intensive attention has been attracted to metasurfaces, a class of planar metamaterials with exceptional abilities to mold light flow.⁸ The central idea of metasurfaces is to introduce the desired phase profile by patterning subwavelength structures at the interface between two natural materials. The rationally designed phase offers an additional, yet a very important degree of freedom to fully control the wave propagation. For instance, anomalous reflection and refraction have been demonstrated in the infrared region.^{9,10} Metasurface-based optical devices, such as vortex plates,¹¹ wave plates,^{12–14} and ultra-thin focusing lenses,^{15,16} have also been realized for different types of incident light, *i.e.*, linearly polarized light, circularly polarized light, or vertex beams.

So far, almost all studies on metasurfaces have focused on manipulating propagating waves. In contrast, only a few of them^{17–20} have been devoted to employing metasurfaces to control near-field waves, such as surface plasmons. Surface plasmons are collective electron density oscillations that are coupled to external light.²¹ They behave optical surface waves propagating along a metal-dielectric interface with field intensity exponentially decaying away from the interface, or they are tightly confined in all three dimensions around a metallic nanostructure. Due to the strong confinement and large field enhancement, surface plasmons promise a variety of applications in super-resolution imaging and lithography, data storage, ultra-compact optical devices, as well as biomedical sensing.^{22–25}

In this letter, we demonstrate that one-dimensional metallic gratings, a simple metasurface with practically feasible geometries, are capable of tailoring the dispersion, and thus the propagation characteristic of surface plasmons in an unprecedented manner.²⁶ The structure is schematically shown in Fig. 1, where a grating pattern (with width w , height h , and period p) is carved into a metal. It is found that the constant frequency contour of surface plasmons can be tuned from being convex to flat, and to hyperbolic. As a result, normal, non-divergent and anomalous diffraction are achieved as surface plasmons propagate along the metasurface. In particular, arising from the hyperbolic constant frequency contour, surface plasmons undergo negative refraction as they propagate from a flat metal surface to a metasurface. These findings open an innovative avenue to designing on-chip plasmonic devices for imaging, light concentration, biosensing, and optical communication.

We start with studying the plasmonic mode of a single metallic ridge, in order to understand the mechanism of the metasurface consisting of an array of ridges. Previous work showed that a metallic ridge supports a plasmon mode that has electric field tightly confined on the top of the ridge.²⁷ Using a commercial finite-element analysis software

^{a)}Electronic mail: xiang@berkeley.edu

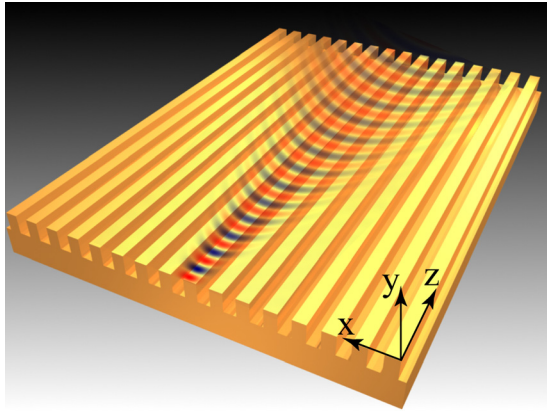


FIG. 1. Schematic illustration of a metasurface made of periodic metallic gratings, which supports surface plasmons propagation with a hyperbolic phase front.

(Comsol Multiphysics 4.3a), we simulate the mode profile of a single silver ridge of width $w = 60$ nm and $h = 80$ nm, as shown in Fig. 2. The permittivity of silver is described by the Drude model $\epsilon_m(\omega) = \epsilon_\infty - \frac{\omega_p^2}{\omega(\omega + i\gamma_c)}$, where the high-frequency bulk permittivity $\epsilon_\infty = 6$, the bulk plasmon frequency $\omega_p = 1.5 \times 10^{16}$ rad/s, and the collision frequency $\gamma_c = 7.73 \times 10^{13}$ rad/s are obtained by fitting the experimental data from the literature.²⁸ At the wavelength of 543 nm, the effective mode index of the ridge plasmon mode, defined as $n_{eff} = k_{z,sp}/k_0$, is equal to $1.087 + 0.0057i$. For comparison, the effective mode index of surface plasmons on a flat semi-infinite silver-air interface is $1.045 + 0.002i$, which is smaller than the mode index of the ridge plasmon mode. Therefore, surface plasmons can be well confined on the ridge, without being decoupled to the plasmon mode on the flat silver-air interface. It should be noted that the ridge plasmon mode is not sensitive to the deformation of the

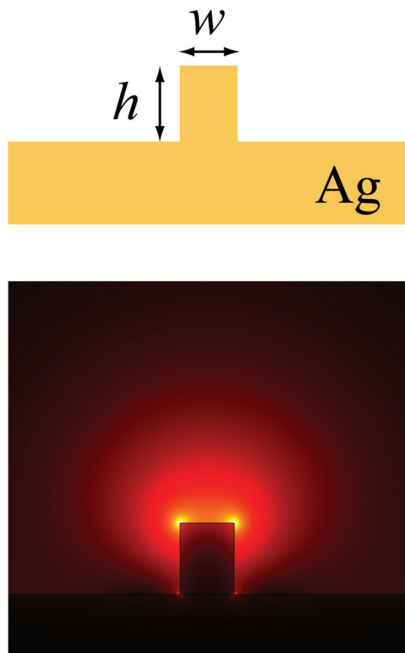


FIG. 2. Electric field intensity ($|E|$) distribution of the plasmon mode on a single silver grating ($w = 60$ nm and $h = 80$ nm) at the wavelength of 543 nm. The field is strongly confined at the top of the silver ridge.

geometry, such as curved corners and non-vertical side walls. This unique characteristic is confirmed from the field distribution and the mode index calculation for the two non-ideal structures. Meanwhile, the effective index of the ridge plasmon mode is larger than that of surface plasmons on a flat silver-air interface at the same wavelength over a broad spectral spectrum, which guarantees the confinement of surface plasmons on the ridge.²⁹ Therefore, ridge plasmon modes are a good candidate for practical wave guiding and light confinement at deep subwavelength scales. The metasurface constructed by an array of ridges is expected to be insensitive to fabrication imperfections, ideal for studying surface plasmons propagating on the metasurface.

When an array of ridges is periodically arranged (with periodicity p) to form a metasurface, the plasmon mode on each ridge is coupled, or hybridized, through evanescent wave coupling. All the allowed plasmon modes comprise a band. Figure 3 plots the effective mode index of the coupled plasmon modes, both real part and imaginary part, at three different wavelengths ($\lambda_0 = 633$ nm, 543 nm, and 500 nm). In the first Brillouin zone ($-\pi/p \leq k_x \leq \pi/p$), the constant frequency contour (*i.e.*, dependence of the real part of n_{eff} versus the transverse momentum k_x) shown in Fig. 3(a) exhibits distinct differences. When the wavelength is 500 nm, n_{eff} is maximum at the edge of Brillouin zone ($k_x = \pm\pi/p$), while it is minimum at the Brillouin center ($k_x = 0$). Overall, the constant frequency contour is hyperbolic, except near the edge of the Brillouin zone. As a result, the curvature of the plasmon mode band (*i.e.*, the second derivative) is positive at $k_x = 0$, and negative at $k_x = \pi/p$, indicating that the diffraction of a wave packet is anomalous at $k_x = 0$ and normal at $k_x = \pi/p$.³⁰ In contrast, the reversed characteristics are observed at $\lambda_0 = 633$ nm, where the constant frequency contour has a convex shape. Very interestingly, the plasmon mode band for 543 nm wavelength is almost flat, implying the diffraction can be suppressed as surface plasmons propagate along the metasurface. Figure 3(b) plots the imaginary part of the mode index, which always gradually increases when $|k_x|$ increases. This is because for larger $|k_x|$, more fields penetrate into the metal, and hence more energy dissipates into heat.

Mathematically, the difference of the constant frequency contour can be understood from the coupled mode theory that has been applied to study the interaction of photonic modes in dielectric waveguide arrays.³¹ In an array of waveguides, the propagation constant along z-axis is given by $k_z = \beta + 2C \cos(k_x p)$, where β is a constant, and C is the

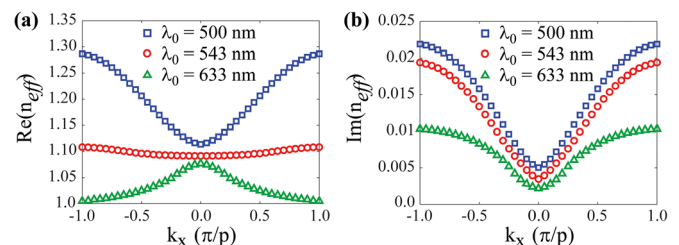


FIG. 3. (a) Real and (b) imaginary part of the mode index for surface plasmons on a metasurface consisting of periodic silver gratings at different wavelengths. The geometric parameters of the grating are $p = 120$ nm, $w = 60$ nm, and $h = 80$ nm.

coupling coefficient between photonic modes. Apparently, the curvature of the constant frequency contour depends on the sign of the coupling coefficient. For dielectric waveguide arrays, the coupling coefficient is commonly positive. The propagation constant, thus effective mode index for the first band is maximum at $k_x=0$, which is also valid for the plasmon mode on the metasurface at 633 nm wavelength. However, the situation changes for the same metasurface when the wavelength is reduced to 500 nm, where the coupling coefficient becomes negative and the constant frequency contour has a minimum at $k_x=0$. There is a transition point where the coupling coefficient is almost zero, leading to a propagation constant independent on k_x (*i.e.*, a flat band). We can understand why the coupling coefficient changes signs in the following way. At short wavelength, the plasmon mode is strongly confined. Therefore, the metallic grating can be considered as a metal-dielectric multilayer supporting hyperbolic constant frequency contour.³² However, the field is much less confined at a longer wavelength, and consequently the surface morphology modulation is not sufficient to reverse the shape of the constant frequency contour. These results strongly indicate that we can readily engineer the coupling coefficients and constant frequency contour for surface plasmons on the metasurface, depending on the wavelength and geometrical parameters.

Three-dimensional full-wave simulations (CST Microwave Studio) taking into account the realistic geometry confirm the different propagation characteristics as surface plasmons propagate on a metasurface. In the simulation, a small waveguide port is placed adjacent to the metasurface, which is constructed by milling periodic grooves into an optically thick silver film. Plasmon modes are excited by the port and propagate along the z -axis. Figure 4 shows the y -component of the electric field (E_y) in the plane 5 nm above the metasurface. Although the electric field shows discretized features due to the surface topography, we can clearly visualize that the phase front of surface plasmons on the metasurface is concave, flat, and convex at the wavelength of 500 nm, 543 nm, and 633 nm, respectively, arising from the different curvature of constant frequency contours shown in Fig. 3(a). At 500 nm wavelength, surface plasmons are focused when they reach the flat silver interface region (top

region in Fig. 4(a)), clearly showing that metasurface can be used as a planar imaging device. Remarkably, at 543 nm wavelength, surface plasmons do not diverge after propagating 4 μm , although the beam width is only about 300 nm. Such a self-focusing effect may be very useful for designing surface hyperlens as *conceptually* proposed in Ref. 8, as well as light harvesting from nano-emitters to improve the emission directionality and collection efficiency.

We intend to propose a feasible geometry of metasurface for manipulating surface plasmons. Therefore, the period of the grating ($p=120$ nm) considered in Figs. 3 and 4 is not deep subwavelength, but still four-fold smaller than the shortest wavelength (500 nm). Such a length scale satisfies the conventional requirement of metamaterials. Owing to the periodicity, the deviation of the constant frequency contour from a hyperbola does exist near the edge of the Brillouin zone ($|k_x| \approx \pi/p$) at 500 nm wavelength. The central region of the constant frequency contour ($|k_x| \leq \pi/2p$), however, can be still considered as a good approximation of an effective medium in the context of metamaterials. In fact, it is claimed that the effective medium method can work up to the Wood anomaly, where the wavelength is comparable to the periodicity and diffraction starts to occur. Under this condition, the periodic structure can no longer be considered a homogeneous effective material.³³ Apparently, our current design is away from the Wood anomaly. To ease potential difficulties in the fabrication, we have designed metasurfaces with a larger periodicity and a smaller aspect ratio,²⁹ which show similar results as Figs. 3 and 4.

The hyperbolic constant frequency contour enables all-angle and broadband negative refraction for surface plasmons. The group velocity, defined as $\bar{v}_g = \nabla_{\vec{k}} \omega$, lie normal to the constant frequency contour.³² Therefore, the group velocity of surface plasmons on metasurfaces is negative when the constant frequency contour is hyperbolic. If surface plasmons are launched from a flat metal interface, on which group velocity of surface plasmons is positive, surface plasmons will encounter negative refraction right after passing the metasurface. Such negative refraction of surface plasmons, confined to the two dimensions, is the counterpart of the negative refraction of freely propagating waves utilizing bulk hyperbolic metamaterials.^{32,34,35} Figure 5 presents the

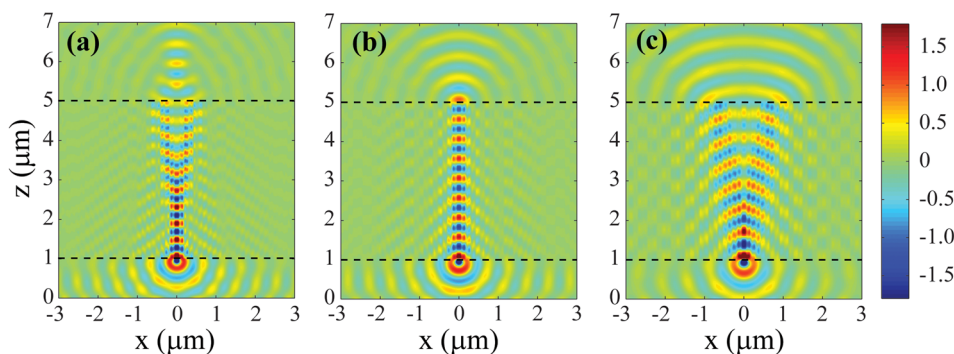


FIG. 4. Propagation of surface plasmons along the metasurface at three different wavelengths (a) 500 nm, (b) 543 nm, and (c) 633 nm, exhibiting anomalous, non-divergent, and normal diffraction, respectively. Here, we plot the snapshot of the y component of the electric field (E_y) at the plane 5 nm above the metasurface. The region between the two dashed lines is metasurface, while the remaining is flat silver-air interface. The geometric parameters of the grating in the metasurface region are $p=120$ nm, $w=60$ nm, and $h=80$ nm.

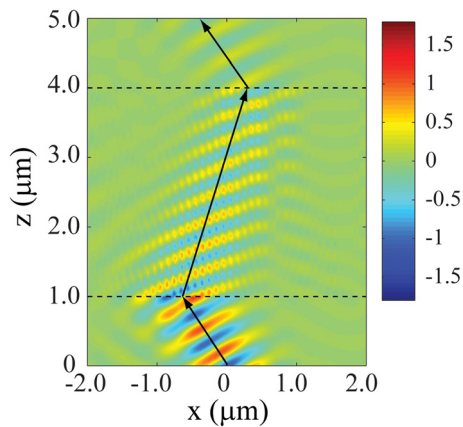


FIG. 5. Negative refraction of surface plasmons at the wavelength of 458 nm, when surface plasmons are incident from a flat silver-air interface to a metasurface. Here, we plot the snapshot of the y component of the electric field (E_y) at the plane 5 nm above the metasurface. The region between the two dashed lines is metasurface, while the remaining is flat silver-air interface. The geometric parameters of the grating in the metasurface region are $p = 100$ nm, $w = 40$ nm, and $h = 100$ nm. Compared with Figs. 3 and 4, a smaller periodicity and larger aspect ratio used here result in more pronounced negative refraction of surface plasmons.

full-wave simulation result at the plane 5 nm above the metasurface for a grating with $p = 100$ nm, $w = 40$ nm, and $h = 100$ nm at the wavelength 458 nm. The smaller periodicity, larger grating aspect ratio, and shorter wavelength lead to a steeper slope of the constant frequency contour, producing more pronounced negative refraction of surface plasmons. The incident angle of surface plasmons is 30° , and the resulting refraction angle is about -15° , in good agreement with the estimation from the constant frequency contour. It can be seen that the power flow (group velocity) undergoes negative refraction, while the wave vector (phase velocity) remains positive direction. This phenomenon is due to the strong anisotropy of the metasurface.^{34,35} Owing to the hyperbolic constant frequency contour, negative refraction of surface plasmons take place for all incident angles. Moreover, it can work over a broad wavelength range as indicated by the evolution of constant frequency contours shown in Fig. 3. Such a simple metasurface platform provides considerable advantages for bending surface plasmons negatively, compared with previous work based on gap plasmons in a metal-dielectric-metal geometry.³⁶ Finally, it is fundamentally different from negative refraction in photonic crystals, which works near the edge of Brillouin zone or high-order band where diffraction plays an important role. In contrast, the negative refraction in our metasurface design works in the subwavelength region. The simulation of the band structure and negative refraction in a disordered grating further confirms the difference.²⁹

In conclusion, we show that a metasurface made of periodic metallic gratings can drastically modify the dispersion of surface plasmons, giving rise to flat or hyperbolic constant frequency contour that are distinctly different from that of surface plasmons on an unstructured metal surface. As a result, non-divergent diffraction, anomalous diffraction, and negative refraction of surface plasmons have been numerically demonstrated. It is anticipated that these results can be readily confirmed in experiments, based on our designed

metasurfaces with practical geometries. Our findings substantially extend the concept of metasurfaces into the near field region, and hold promising applications on a planar photonic footprint. For instance, the hyperbolic constant frequency contour implies enhanced photonic density of states, which can significantly increase emitter's decay rate.^{8,37} The metasurface also provides a unique platform to explore the spin and orbit angular momentum of light for information processing and communication.^{18,38,39} Last but not least, similar strategies can be applied to spoof surface plasmons at microwave and terahertz region,⁴⁰ where metals are essentially perfect conductors and unable to support surface plasmons.

This work was supported by the U.S. ARO MURI program (W911NF-09-1-0539).

- ¹D. Smith, J. Pendry, and M. Wiltshire, *Science* **305**, 788 (2004).
- ²Y. Liu and X. Zhang, *Chem. Soc. Rev.* **40**, 2494 (2011).
- ³C. M. Soukoulis and M. Wegener, *Nat. Photonics* **5**, 523 (2011).
- ⁴R. Shelby, D. Smith, and S. Schultz, *Science* **292**, 77 (2001).
- ⁵S. Xi, H. Chen, T. Jiang, L. Ran, J. Huangfu, B.-I. Wu, J. A. Kong, and M. Chen, *Phys. Rev. Lett.* **103**, 194801 (2009).
- ⁶J. B. Pendry, D. Schurig, and D. R. Smith, *Science* **312**, 1780 (2006).
- ⁷U. Leonhardt, *Science* **312**, 1777 (2006).
- ⁸A. V. Kildishev, A. Boltasseva, and V. M. Shalaev, *Science* **339**, 6125 (2013).
- ⁹N. Yu, P. Genevet, M. A. Kats, F. Aieta, J.-P. Tetienne, F. Capasso, and Z. Gaburro, *Science* **334**, 333 (2011).
- ¹⁰X. Ni, N. K. Emani, A. V. Kildishev, A. Boltasseva, and V. M. Shalaev, *Science* **335**, 427 (2012).
- ¹¹P. Genevet, N. Yu, F. Aieta, J. Lin, M. A. Kats, R. Blanchard, M. O. Scully, Z. Gaburro, and F. Capasso, *Appl. Phys. Lett.* **100**, 013101 (2012).
- ¹²E. H. Khoo, E. P. Li, and K. B. Crozier, *Opt. Lett.* **36**, 2498 (2011).
- ¹³Y. Zhao and A. Alù, *Phys. Rev. B* **84**, 205428 (2011).
- ¹⁴N. Yu, F. Aieta, P. Genevet, M. A. Kats, Z. Gaburro, and F. Capasso, *Nano Lett.* **12**, 6328 (2012).
- ¹⁵A. Pors, M. G. Nielsen, R. L. Eriksen, and S. I. Bozhevolnyi, *Nano Lett.* **13**, 829 (2013).
- ¹⁶X. Chen, L. Huang, H. Mühlenbernd, G. Li, B. Bai, Q. Tan, G. Jin, C.-W. Qiu, S. Zhang, and T. Zentgraf, *Nat. Commun.* **3**, 1198 (2012).
- ¹⁷S. Sun, Q. He, S. Xiao, Q. Xu, X. Li, and L. Zhou, *Nature Mater.* **11**, 426 (2012).
- ¹⁸P. Genevet, J. Lin, M. A. Kats, and F. Capasso, *Nat. Commun.* **3**, 1278 (2012).
- ¹⁹J. Lin, J. B. Mueller, Q. Wang, G. Yuan, N. Antoniou, X.-C. Yuan, and F. Capasso, *Science* **340**, 331 (2013).
- ²⁰L. Huang, X. Chen, B. Bai, Q. Tan, G. Jin, T. Zentgraf, and S. Zhang, *Light: Sci. Appl.* **2**, e70 (2013).
- ²¹H. Raether, *Surface Plasmons* (Springer, Berlin, 1988).
- ²²W. L. Barnes, A. Dereux, and T. W. Ebbesen, *Nature* **424**, 824 (2003).
- ²³J. A. Schuller, E. S. Barnard, W. Cai, Y. C. Jun, J. S. White, and M. L. Brongersma, *Nature Mater.* **9**, 193 (2010).
- ²⁴N. J. Halas, *Nano Lett.* **10**, 3816 (2010).
- ²⁵H. Choi, D. F. Pile, S. Nam, G. Bartal, and X. Zhang, *Opt. Express* **17**, 7519 (2009).
- ²⁶Y. M. Liu, "Plasmonic metamaterials," Ph.D. dissertation (University of California at Berkeley, 2009).
- ²⁷E. Vesseur, R. De Waele, H. Lezec, H. Atwater, F. G. de Abajo, and A. Polman, *Appl. Phys. Lett.* **92**, 083110 (2008).
- ²⁸P. B. Johnson and R. Christy, *Phys. Rev. B* **6**, 4370 (1972).
- ²⁹See supplementary material at <http://dx.doi.org/10.1063/1.4821444> for plasmon mode profile of ridges with deformed geometries, as well as the band structure and negative refraction of surface plasmons in a disordered grating.
- ³⁰Y. Liu, G. Bartal, D. A. Genov, and X. Zhang, *Phys. Rev. Lett.* **99**, 153901 (2007).
- ³¹H. Eisenberg, Y. Silberberg, R. Morandotti, and J. Aitchison, *Phys. Rev. Lett.* **85**, 1863 (2000).
- ³²X. Fan, G. P. Wang, J. C. W. Lee, and C. Chan, *Phys. Rev. Lett.* **97**, 73901 (2006).

- ³³T. Ergin, N. Stenger, P. Brenner, J. B. Pendry, and M. Wegener, *Science* **328**, 337 (2010).
- ³⁴J. Yao, Z. Liu, Y. Liu, Y. Wang, C. Sun, G. Bartal, A. M. Stacy, and X. Zhang, *Science* **321**, 930 (2008).
- ³⁵Y. Liu, G. Bartal, and X. Zhang, *Opt. Express* **16**, 15439 (2008).
- ³⁶H. J. Lezec, J. A. Dionne, and H. A. Atwater, *Science* **316**, 430 (2007).
- ³⁷Z. Jacob, J.-Y. Kim, G. Naik, A. Boltasseva, E. Narimanov, and V. Shalaev, *Appl. Phys. B* **100**, 215 (2010).
- ³⁸N. Shitrit, I. Bretner, Y. Gorodetski, V. Kleiner, and E. Hasman, *Nano Lett.* **11**, 2038 (2011).
- ³⁹X. Yin, Z. Ye, J. Rho, Y. Wang, and X. Zhang, *Science* **339**, 1405 (2013).
- ⁴⁰J. Pendry, L. Martin-Moreno, and F. Garcia-Vidal, *Science* **305**, 847 (2004).